Heliyon 10 (2024) e26391

Contents lists available at ScienceDirect

Heliyon

journal homepage: www.cell.com/heliyon

Research article

Restricted diffusion characteristics in oscillating gradient spin echo with mesoscopic phantom

Hinako Oshiro [a,b], Junichi Hata [a,b,c,d,*], Daisuke Nakashima [c], Rintaro Oshiro [e], Naoya Hayashi [a,b], Yawara Haga [b,c], Kei Hagiya [b], Daisuke Yoshimaru [b,c,d], Hideyuki Okano [b,c]

[a] Graduate School of Human Health Sciences, Tokyo Metropolitan University, Tokyo, Japan
[b] RIKEN, Center for Brain Science, Wako, Saitama, Japan
[c] Keio University, School of Medicine, Tokyo, Japan
[d] Division of Regenerative Medicine, The Jikei University School of Medicine, Tokyo, Japan
[e] Department of Physics, Faculty of Science and Technology, Keio University, Japan

ARTICLE INFO

Keywords:
Diffusion spectrum
Mesoscopic phantom
B-value dependence
Oscillating gradient spin echo
Restricted diffusion
Diffusion MRI

ABSTRACT

In diffusion magnetic resonance imaging, oscillating gradient spin echo (OGSE) has an extremely short diffusion time if motion probing gradient (MPG) is applied to the waveform. Further, it can detect microstructural specificity. OGSE changes sensitivity to spin displacement velocity based on the MPG phase. The current study aimed to investigate the restricted diffusion characteristics of each OGSE waveform using the capillary phantom with various b-values, frequencies, and MPG phases. We performed OGSE (b-value = 300, 500, 800, 1200, 1600, and 2000 s/mm^2) for the sine and cosine waveforms using the capillary phantom (6, 12, 25, 50, and 100 μm and free water) with a 9.4-T experimental magnetic resonance imaging system and a solenoid coil. We evaluated the axial and radial diffusivity (AD, RD) of each structure size. The output current of the MPG was assessed with an oscilloscope and analyzed with the gradient modulation power spectra by fast Fourier transform.

In sine, the sidelobe spectrum was enhanced with increasing frequency, and the central spectrum slightly increased. The difference in RD was detected at 6 and 12 μm; however, it did not depend on the structure scale at 50 or 100 μm and free water. In cosine, the diffusion spectrum was enhanced, whereas the central spectrum decreased with increasing frequency. Both AD and RD in cosine had a frequency dependence, and AD and RD increased with a higher frequency regardless of structure size. AD and RD in either sine or cosine had no evident b-value dependence. We evaluated the OGSE-restricted diffusion characteristics. The measurements obtained diffusion information similar to the pulsed gradient spin echo. Hence, the cosine measurements indicated that a higher frequency could capture faster diffusion within the diffusion phenomena.

* Corresponding author. Graduate School of Human Health Sciences, Tokyo Metropolitan University, 7-2-10 Higashi-Ogu, Arakawa-ku, Tokyo, 116-8551, Japan.
E-mail address: j-hata@tmu.ac.jp (J. Hata).

https://doi.org/10.1016/j.heliyon.2024.e26391
Received 12 January 2023; Received in revised form 4 February 2024; Accepted 12 February 2024
Available online 18 February 2024

Abbreviations

dMRI	diffusion MRI
DTI	diffusion tensor imaging
MSD	root mean square displacement
PGSE	pulsed gradient spin echo
PGSTE	pulsed gradient stimulated echo
OGSE	oscillating gradient spin echo
MPG	motion probing gradient
N	number of lobes
NMR	Nuclear Magnetic Resonance
AD	axial diffusivity
RD	radial diffusivity

1. Introduction

In diffusion magnetic resonance imaging (dMRI), the diffusion coefficients, calculated via diffusion tensor imaging (DTI), represents the direction and velocity of water molecules diffusing in the measured object [1,2]. Diffusion of water molecules occurs via the Brownian motion, and the diffusion coefficient decreases when the random walk is inhibited. Further, the diffusion coefficient in restricted structures decreases based on the structural scale, and its use for estimating axon diameter [3,4] and neuronal microstructure was investigated [5,6].

Setting the diffusion time adjusts the sensitivity of the water molecule diffusion distance in the target for dMRI measurement. The diffusion time is similar to the sampling interval of random spin displacements [7,8]. Selecting an appropriate diffusion time to suit the structural scale can detect specificity in the uniform tissue. The theoretical diffusion time required for estimating structure can be calculated from the root mean square displacement (MSD) [9]. Therefore, diffusion time is essential for the adequate evaluation of the structural scale.

In time-dependent dMRI, pulsed gradient spin echo (PGSE) and pulsed gradient stimulated echo (PGSTE), commonly used, have diffusion times of 10–1000 ms. In this case, the target structural scales are large cells ($>$10 μm), such as hepatocytes [10] and myocytes [11] in vivo. By contrast, microstructures, including neural cells measuring 0.1–10 μm, are defined as a mesoscopic scale [12], and require an extremely short diffusion time (a few ms) to distinguish the restricted diffusion in such tissue microstructural differences. The shortest diffusion time achieved with PGSE and PGSTE with maintaining the b-value is based on the maximum gradient field strength of the MRI scanner. It is not suitable for mesoscopic scale measurements requiring a diffusion time of $\leq$10 ms for structure estimation [13].

Oscillating gradient spin echo (OGSE) can have an extremely short diffusion time if motion probing gradient (MPG) is applied to the waveform [14,15]. In OGSE, the frequency components of gradient modulation power spectra are based on the phase of the applied waveform, and they change the sensitivity to spin displacement velocity [16]. If the phase is applied in the cosine waveform, the sidelobe spectrum (F(ω)) component is large and sensitive to restricted diffusion, thereby obtaining data without flow effects. Conversely, if the phase is applied in the sine waveform, the gradient modulation power spectra emphasize on the central spectrum ($\omega = 0$, F(0)) as well as the sidelobe spectrum. Therefore, data can reflect diffusion and flow phenomena. The gradient modulation power spectra in PGSE comprise a Gaussian distribution centered on the zero range, and similar diffusion information in PGSE is obtained by setting the phase sine in OGSE.

The parameters of OGSE are similar to those of PGSE except for the frequency of the applied waveform. The frequency is determined by setting the number of lobes (N), which represents the total count of lobes in the MPG. Previous studies [4,17] have shown that a greater frequency achieved by increasing N results in a higher sensitivity to diffusion phenomenon and increases diffusion coefficients. However, in OGSE, there is a limit to the maximum N that can be set with a maintaining constant b-value according to the magnetic field strength of the device. Further, the frequency dependence of the diffusion coefficients has yet to be investigated in detail. In previous studies using OGSE [18–21], the number of N was commonly set to 2–3. However, the frequency set by several N is not enough to obtain high-sensitivity diffusion measurements at a high-frequency range. The maximum N number that can be set depends on the b-value. The effect of N and b-value settings on the diffusion coefficients has been predicted via simulation only [17]. However, to our knowledge, no previous study has evaluated actual measurements using a uniform structure, such as a phantom. Nuclear magnetic resonance (NMR) diffusion measurements in cells suggest that diffusion time-dependent measurements $<$1 ms with varying b-values are applicable to the probing of biophysical processes by cellular organelles [18]. The clarification of the diffusion coefficient dependence on the b-value in OGSE could provide essential information to help understand the characteristics of OGSE and set up the OGSE sequence parameters.

Phantom studies in OGSE have been water or solution filled [19–23] and have bead samples [14–16]. These studies can provide information on mixed free and restricted diffusion structures and do not reflect diffusion only in the restricted structure. Most previous studies on OGSE currently focus on diffusion in multiple compartment spaces and have not evaluated the restricted diffusion characteristics in the single component. The capillary plates used in this study have no water molecules outside the restricted structure. They reflect the single-component water molecule diffusion dynamics, enabling a detailed evaluation of sensitivity to restricted

diffusion.

This study aimed to investigate the dependence of OGSE on structure size, b-value, and frequency based on various b-values and by setting N widely in several capillary plate sizes. The measured radial diffusivity (RD), a minimal transfer of water molecules, is used to characterize restricted diffusion in OGSE. When comparing the changes in diffusion characteristics of a single component in different sequence conditions, we evaluated the basic diffusion properties in OGSE and found that they support the arguments of previous studies.

2. Material and methods

2.1. Capillary phantom

The capillary plate (Hamamatsu Photonics, Japan) is a 2-mm-thick lead glass plate with circular holes drilled to a pore size ratio of >55%, and has a two-dimensional array of water-impermeable capillaries (Fig. 1). We observed capillary plates of each size with a phase contrast microscope (BZ-X710, KEYENCE, Japan) using a Plan Fluorite 20 × objective lens (NA0.45, BZ-PF20LP, KEYENCE, Japan). In this study, we prepared two plates, each with pore sizes of 6, 12, 25, 50, and 100 μm. Two 1-mm resin spacers were placed between each size plate and filled with pure water in a centrifuge tube (Iwaki, Japan) with an inner diameter of 29 mm, vacuum degassed the phantom. The effect of the remaining air was eliminated via measurement after at least 2 months of permeation time after sealing. The area of the phantom without the capillary plate was measured as free water.

We performed multi axis imaging for the application of OGSE to biological models in this study. By measuring the diffusion in all directions at once and analyzing the diffusion in the short-axis direction of the capillary with the tensor, the data obtained are highly reproducible and accurate.

2.2. MRI protocol

MRI was performed using a 9.4-T system (660 mT/m, Bruker Biospin, Germany) and a solenoid coil with a 28-mm inner diameter (Takashima Seisakusyo, Japan). We performed OGSE with the following parameters: sine and cosine waveforms; repetition time, 5000 ms; echo time, 70 ms; field of view, 32 × 32 mm^2; matrix size, 32 × 32; resolution 1.0 × 1.0 mm^2; slice thickness, 2.0 mm; number of averages, 3; gradient duration, 30 ms; gradient separation, 35 ms; diffusion directions, 12; b-value, 300, 500, 800, 1200, 1600, and 2000 s/mm^2; the number of lobes, 1–14 (sine), 1–8 (cosine); frequency, 33–467 Hz (sine), 33–267 Hz (cosine) in 33.33-Hz increments; acquisition time, 1 h and 45 min per one condition (one N); and total acquisition time, 134 h and 45 min. Imaging was performed twice at room temperature (20 °C).

2.3. Data analysis

Data were obtained via diffusion tensor analysis using the Diffusion Toolkit [23], and eigenvalues (λ_1, λ_2, and λ_3) were calculated. In this study, the axial diffusivity (AD = λ_1), the direction of diffusion parallel to the running of the glass tubes in the capillary phantom, RD = ($\lambda_2 + \lambda_3$)/2, and the direction of diffusion orthogonal to the glass tubes were used. The average λ_2 and λ_3 could reduce the difference in eigenvalue repulsion caused by noise [24]. The mean values of circular regions of interest (ROIs) in the phantoms of the

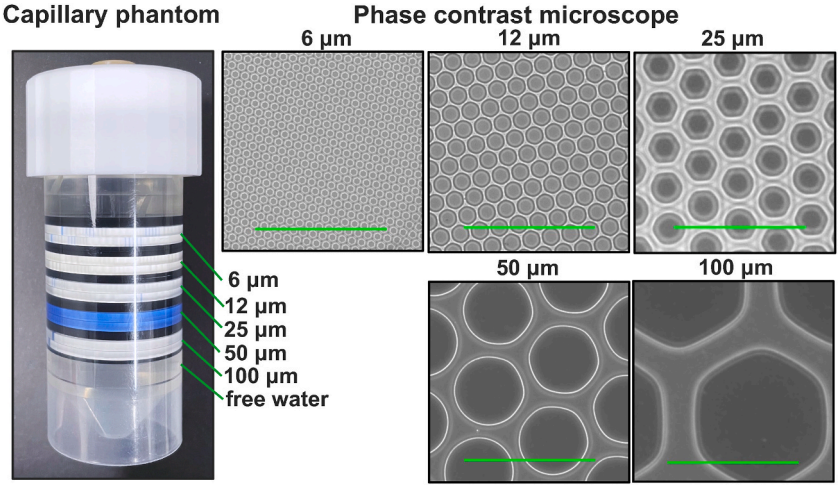

Fig. 1. Capillary phantom. Capillary plates of each size were observed with a phase contrast microscope using a 20 × objective lens (scale bar = 100 μm). We used pore sizes of 6, 12, 25, 50, and 100 μm. In this study, the area in the phantom without the capillary plates was measured as free water.

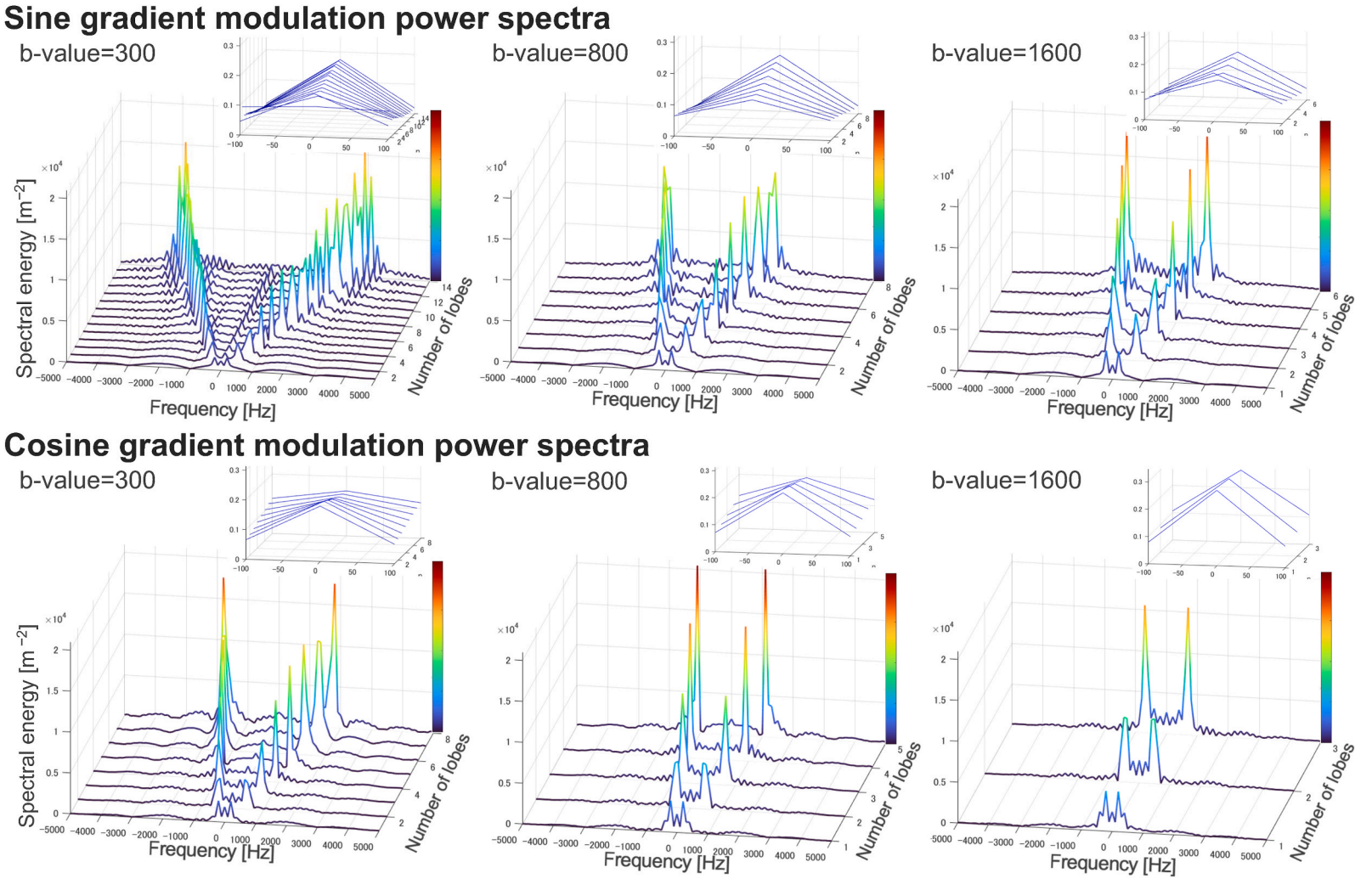

Fig. 2. The gradient modulation power spectra for the number of lobes (N) at b-values of 300, 800, and 1600 s/mm^2. The upper right portion of each graph shows an expanded view of the central spectrum. The sine data in the upper row and cosine data in the lower row for b-values of 300, 800, and 1600 s/mm^2 from left to right in each row. The color bar range corresponds to the absolute value of the spectral intensity. As the b-value increases, the maximum N that can be set decreases. (For interpretation of the references to color in this figure legend, the reader is referred to the Web version of this article.)

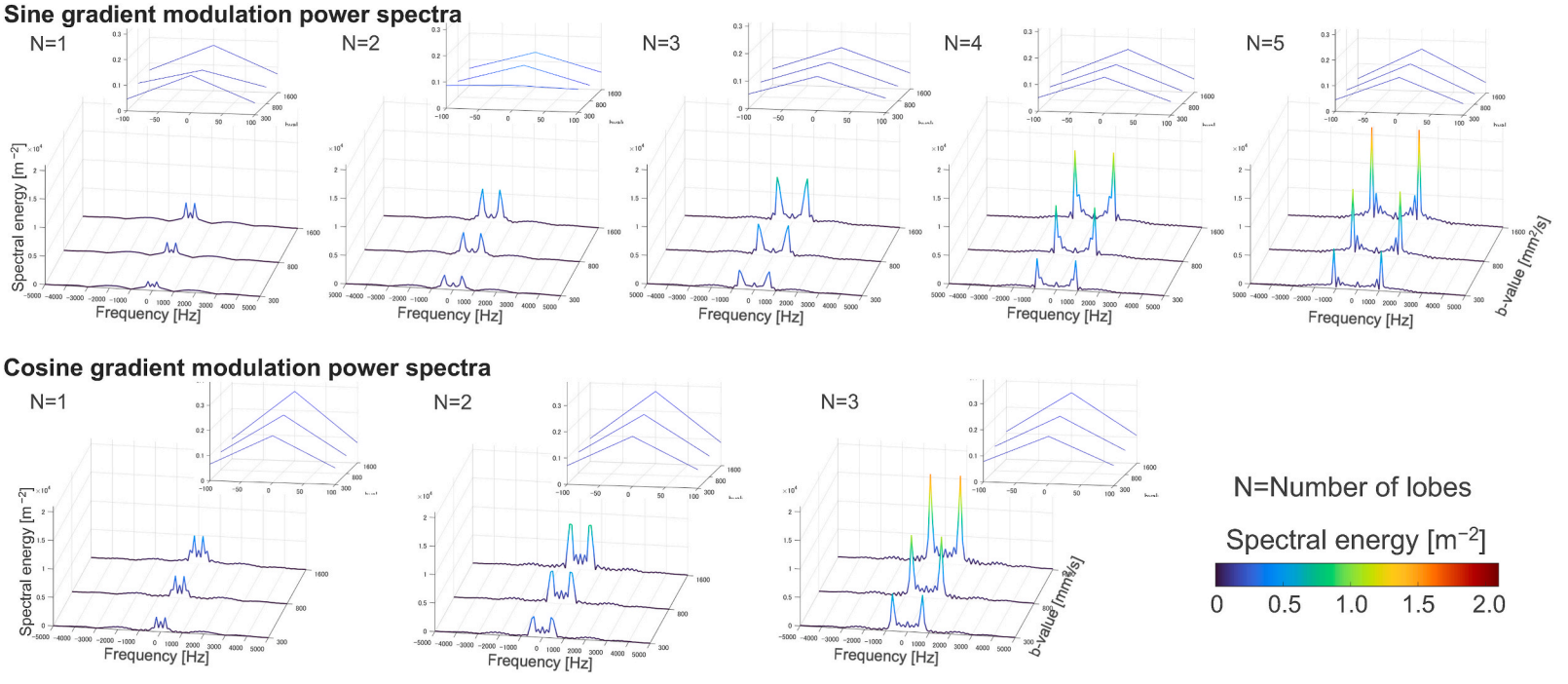

Fig. 3. The gradient power spectra for b-values of 300, 800, and 1600 s/mm^2 at the same number of lobes (N). The upper right portion of each graph shows an expanded view of the central spectrum. The sine in the upper row and cosine in the lower row from the left of each row (N = 1, 2, 3, 4, and 5). The color of each spectrum corresponds to the absolute value of the spectral intensity. (For interpretation of the references to color in this figure legend, the reader is referred to the Web version of this article.)

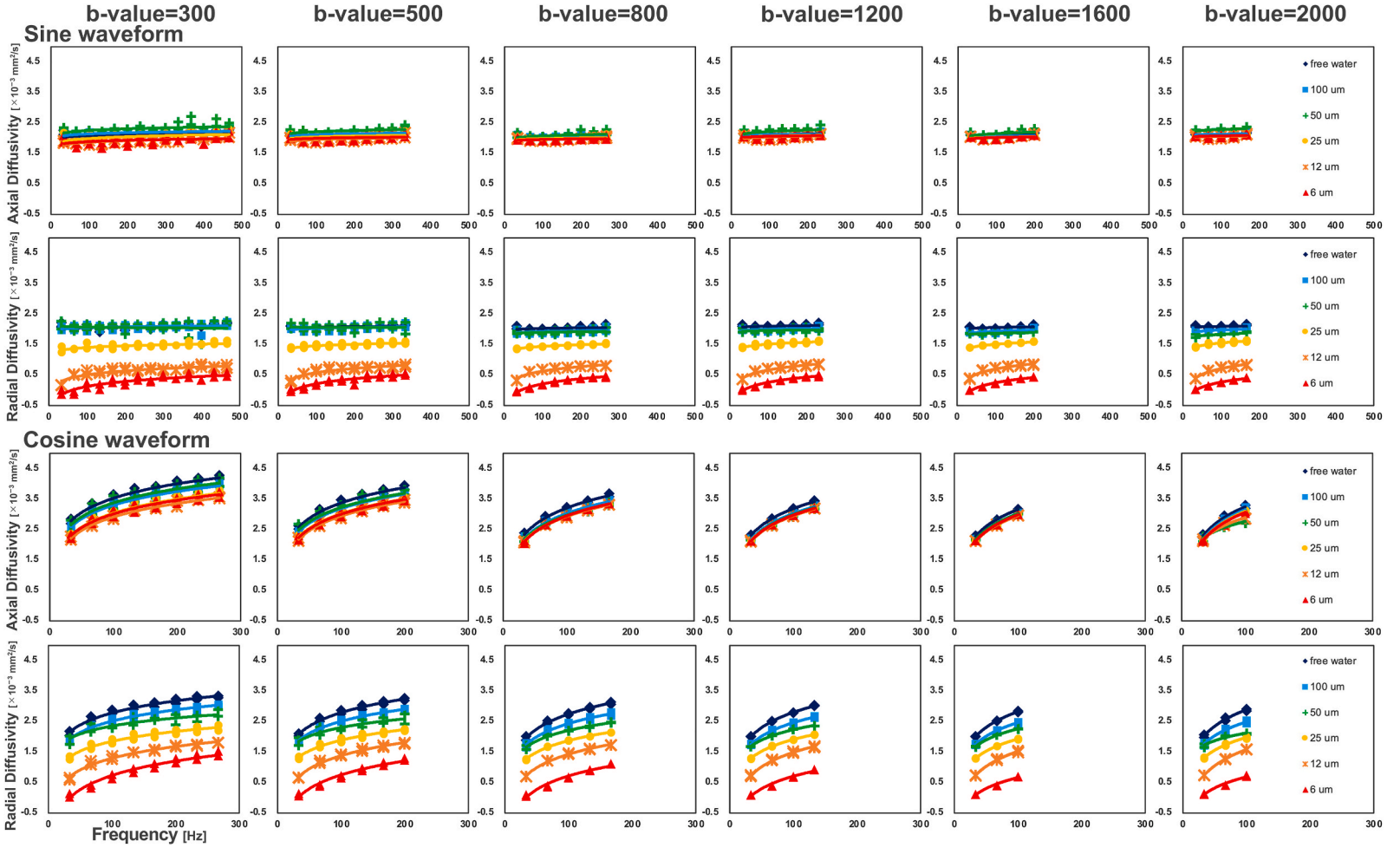

Fig. 4. The axial diffusivity (AD) and radial diffusivity (RD) of the capillary phantom at each b-values are plotted as a function of frequency. AD, RD for sine are presented in the top row and AD, RD for cosine from the left to right in each row, with b-values of 300, 500, 800, 1200, 1600, and 2000 s/mm^2. Two measurement data were plotted and added to the approximate curve obtained from the average value. All graphs are presented as free water (blue), 100 μm (light blue), 50 μm (green), 25 μm (yellow), 12 μm (orange), and 6 μm (red). (For interpretation of the references to color in this figure legend, the reader is referred to the Web version of this article.)

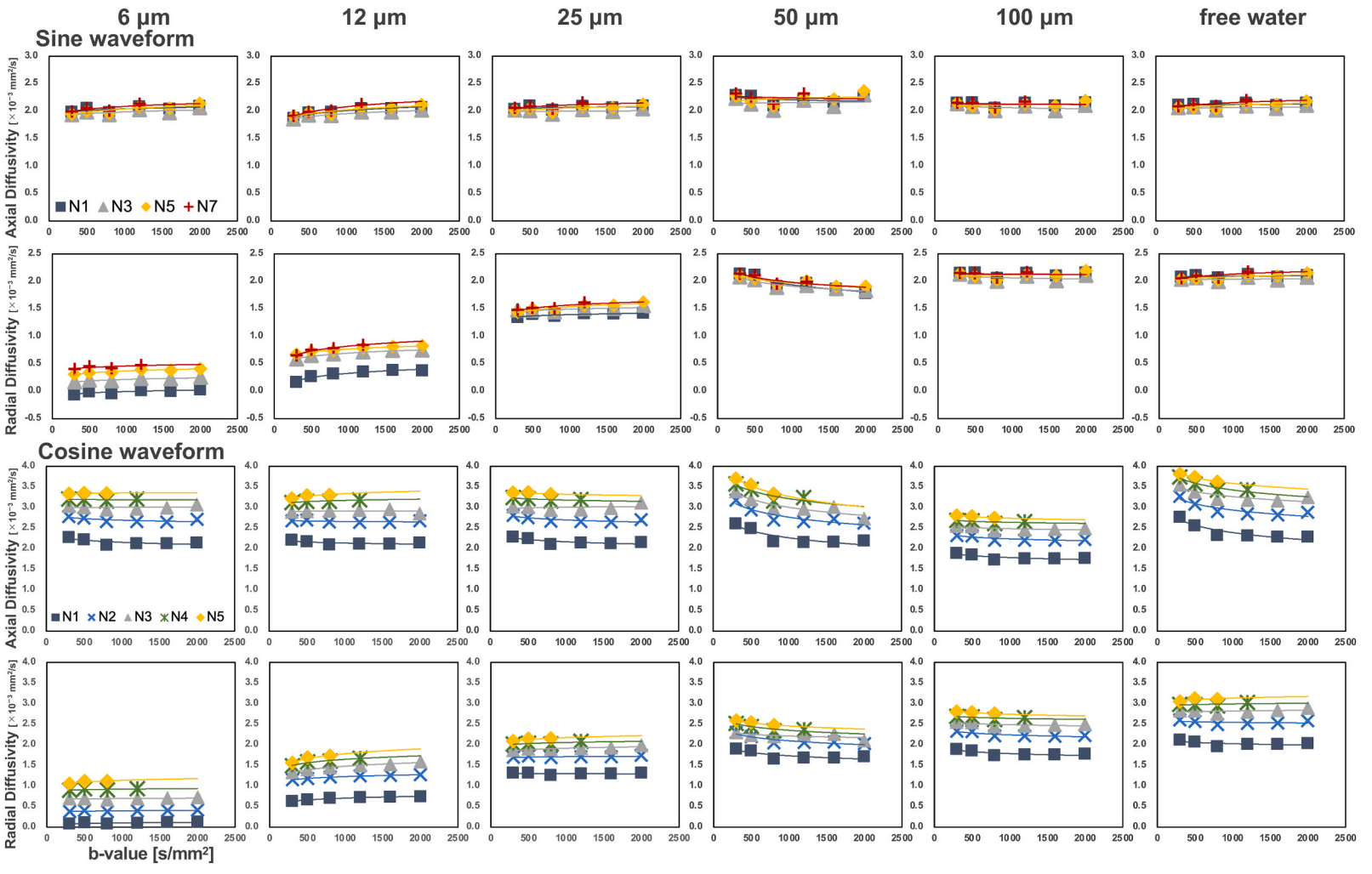

Fig. 5. The axial diffusivity (AD) and radial diffusivity (RD) of the capillary phantom at each structure size are depicted as a function of b-value. AD, RD for sine are presented in the top row and AD, RD for cosine in the left in each row, ordered by structure sizes of 6, 12, 25, 50, and 100 μm and free water. The average value and approximate curve are plotted for the two measurements. For sine, the number of lobes (N) = 1 (navy), 3 (gray), 5 (yellow), and 7 (red); for cosine, N = 1 (navy), 2 (light blue), 3 (gray), 4 (green), and 5 (yellow). (For interpretation of the references to color in this figure legend, the reader is referred to the Web version of this article.)

AD and RD images were measured and plotted on the graphs. Moreover, the output currents of the gradient coil at b-values of 300, 800, and 1600 s/mm^2 were measured using a digital oscilloscope (DS1104Z Plus, RIGOL Technologies, China). The gradient modulation power spectra of the MPG waveforms were analyzed using a fast Fourier transform (MATLAB, version R2021b, MathWorks, the USA).

3. Results

3.1. Gradient modulation power spectra

Fig. 2 shows the gradient modulation power spectra at b-values 300, 800, and 1600 s/mm2 for different frequencies (number of lobes, N) in sine and cosine. The upper right portion of each graph shows an expanded view of the central spectrum. The resulting spectrum was output by Fourier transforming the waveform that was actually used in the measurement, and the waveform included the constant part between the two MPG and crusher gradient. Therefore, the spectral shape differs from the ideal spectral profile suggested in previous studies [16]. The sidelobe spectrum shifted to higher frequencies as N increased because N determines the frequency comprising the sidelobe spectrum. The sidelobe spectrum intensity was enhanced with increasing frequency in both sine and cosine. Although the central spectrum intensity increased slightly at sine with increasing frequency, it decreased at cosine. Fig. 3 shows the spectral intensities at the same N (i.e., frequency) for different b-values (300, 800, and 1600 s/mm^2). In the same frequency, the sidelobe spectrum was enhanced for a larger b-value, and the central spectrum also increased. At the same frequency and with the same b-value, the sidelobe spectral intensity was higher in cosine.

3.2. Diffusion coefficients

The AD and RD transition with frequency changes in the capillary phantom was plotted for each b-value and compared in sine and cosine (Fig. 4). Larger b-values limited the maximum N that could be set, reducing the frequency of the horizontal axis plotted. The AD in sine shows no frequency dependence or structural scale dependence. The RD in sine varied based on the structure scale. At 50, 100 μm, and free water, the frequency did not change and differed in RD. At 6, 12, and 25 μm in sine, RD was distributed according to the structure scale, and it slightly increased to higher frequencies. Similar to the AD in sine, the AD in cosine did not differ with the structural scale. However, it increased with higher frequencies. The result of frequency dependence in the AD is different from that expected from unrestricted axial diffusion. The RD in cosine was distributed according to the structure scale. For all structure scales, the RD increased at higher frequencies.

Fig. 4 was re-plotted as AD and RD transition with b-value changes and regraphed for each structure size (Fig. 5). AD and RD in either sine or cosine had no evident b-value dependence. There was no difference in diffusion coefficient with frequency (N) in AD or RD at 25–100 μm and free water in sine. In RD at 6 and 12 μm, distribution was observed between low frequencies (N1–3). Nevertheless, there was no difference in RD at higher frequencies (N5–7). Both AD and RD had frequency (N) dependence in cosine, and the diffusion coefficient increased with higher frequencies regardless of the structural scale.

Supplemental Fig. 1 shows the AD and RD images at N = 1, 5 for b-value = 800 s/mm^2 in sine and cosine. The mean values and standard deviations measured from a circular ROI placed at the center of the phantom are described in the image. The standard deviation was extremely small in all conditions, and there was no systematic variation depending on imaging parameters (frequency, applied waveform, and pore size) nor on the AD and the RD.

4. Discussion

The current study investigated the transition characteristics of diffusion coefficients in OGSE using multiple sizes of capillary plates with a simple microrestricted structure based on different b-values, frequency (N), and the phase of the applied waveform. The diffusion characteristics of OGSE were considered from the pulse sequence perspective by comparing the gradient modulation power spectrum using the MPG waveform information obtained using the oscilloscope.

4.1. Sine waveform

In sine, the sidelobe spectrum was enhanced with increasing frequency, and the central spectrum slightly increased, confirming that the sine measurement included both diffusion and flow phenomena. A previous study [25] using the same capillary phantom measured with PGSTE showed no diffusion time dependence for AD and free water. The RD was distributed with structure size, indicating that the sine measurement provides diffusion information similar to PGSE. The effective diffusion time in OGSE is estimated by evaluating the b-value formula in PGSE [26], which can be obtained from the frequency (f) with $\Delta_{eff} = 3/8f$. In this study, the sine effective diffusion time was $\Delta_{eff} = 0.8$–11.25 ms, suggesting that we measured restricted diffusion characteristics at an extremely short diffusion time (<10 ms), which cannot be set by PGSTE due to device limitation. Using the Einstein–Smoluchowski equation [9], the root mean square displacement of a water molecule diffusing particles after t [s] in three dimensions was obtained using the following formula: MSD $= \sqrt{6Dt}$. Suppose the equation for the diffusion coefficient of water at 20 °C as $D_{temp20} = 2.0 \times 10^{-9}$ [m^2/s] based on the results of previous studies. In that case [25,27], the time t [s] it takes for water molecules to reach the structural wall can be calculated based on the structural scale. The obtained t [s] represents the theoretical diffusion time required for structure estimation, which is 3.0 ms at 6 μm, 12 ms at 12 μm, and 208 ms at 50 μm. Based on this result, the RD difference at 6 and 12 μm was detected, which could not

be observed with PGSTE. However, no difference was found at 50, 100 μm, and in free water. The extremely short diffusion time (<10 ms) attained by OGSE is not suitable for measuring large structure scales above 50 μm. This result showed that the sine measurement can measure the structural scale dependence in the short diffusion time region, limited by the PGSTE, in accordance with the diffusion theory.

4.2. Cosine waveform

In cosine, the sidelobe spectrum was enhanced and the central spectrum was reduced with increasing frequency, indicating that cosine data reflect the diffusion phenomenon more selectively than the sine data. The AD and free water of RD in cosine increased as compared with the selfdiffusion coefficient of water in a previous study [27]. The sidelobe spectrum becomes narrower and more enhanced with increasing frequency, which reflects the diffusion phenomena more sensitively, resulting in the calculation of larger diffusion coefficients due to the sensitivity to faster diffusion in the diffusion phenomena. Furthermore, the larger difference in RD with structural scale dependence compared with the sine measurement is also explained because there is a greater decrease in the diffusion coefficient as the collision of water molecules with the structural wall contributes to the diffusion velocity by emphasizing on the diffusion phenomena in the cosine measurement. However, previous studies [16,17,26] measuring water phantom in OGSE did not confirm the frequency dependence of the diffusion coefficient in free water, as in our study. One reason is that this study uses a simple cosine waveform, which differs from the cosine modulated waveforms in previous studies. OGSE cosine measurement has an issue, particularly sharp pulse rise. Generally, to address this problem, the cosine modulation waveform replaces the first and last quarter periods with a half period of a sine wave with twice the frequency. The cosine modulation wave reduces eddy currents without strong gradient amplitude requirement. However, cosine modulated waves have the demerit of slightly broadening the peak bandwidth of the sidelobe spectrum compared with the ideal accurate cosine waveform [16]. According to a previous study, the shortest rising time was 0.125 ms if calculated from the frequency using the cosine modulated waveform [16]. In this study, the rising time was 0.15 ms at N = 2 and 0.075 ms at N = 5, calculated based on the oscilloscope result at a b-value of 800 s/mm^2. In this study, an MPG closer to the accurate cosine waveforms was applied at higher frequencies, resulting in greater enhancement of the sidelobe spectrum. The effect of image distortion caused by the eddy current with cosine measurement is considered to be negligible, based on the fact that there was no systematic change in the standard deviation. In general diffusion-weighted imaging, the twisted refocused pulsed echo (TRSE) method [28], in which two pairs of MPG are applied positively and negatively between two 180° pulses, cancels the eddy currents related to the use of MPG. In OGSE, MPG is applied to the positive and negative waveforms as in the TRSE method; thus, the eddy currents cancel out. Therefore, the influence of the eddy current becomes minor in OGSE.

Generally, in addition to eddy current, other causes of image distortion include inhomogeneous magnetic fields and susceptibility artifacts from air in the phantom. However, we performed B0 mapping correction, and no air bubbles were included in the ROIs, so we consider the influence of each of these factors is small. In PGSE, it has been reported that the nonlinearity of the magnetic field gradients causes loss in accuracy of the diffusion tensor as well as image distortion [29,30]. The eigenvalue for PGSE, λ1 is underestimated and λ3 is overestimated in conditions of diffusion gradients inhomogeneity and low SNR. Especially in high-field MRI scanners for research, the dispersion of the eigenvalues caused by magnetic field gradient inhomogeneity has been confirmed as significantly higher [29]. In a previous study using the same 9.4 T-MRI system as our experiment with isotropic water phantoms for DTI measurements, by applying the BSD-DTI (b-matrix spatial distribution in DTI) method, which indicates a b-matrix for each voxel, resulted in dramatic accuracy improvements for determining diffusion coefficients compared to the standard-DTI [30]. The standard deviation of free water in our results decreased by about 84% compared to standard-DTI in all conditions. Meanwhile, compared to after BSD-DTI calibration, our data decreased by about 13% in some conditions, but increased by about 56% in the cosine high-frequency conditions. The increasing trend seems to suggest that the magnetic field gradients linearity was lost with machine loads. As with PGSE, simulations of the influence of diffusion gradients inhomogeneity or sequence specific effects would be future works with OGSE, but the diffusion characteristics of OGSE have been understood through our experiments.

In previous studies using anisotropic phantoms, tensor accuracy is improved by applying BSD-DTI calibration [31]. The capillary phantom used in this study had a standard deviation of <1% of the eigenvalues in the ROI; thus, the phantom was assumed to be homogeneous. In the case of phantoms with low uniformity (standard deviation > 10%) for OGSE imaging, a BSD-DTI calibration may reflect more accurate diffusion information.

The spectrum intensity at the same frequency showed a b-value dependence. However, the diffusion coefficient did not depend clearly on the b-value. Previous studies validated that low b-values (<200 s/mm^2) were affected by microcirculatory flow in OGSE cosine measurements in the mouse brain [20] and that high b-values (>1000 s/mm^2) reduced signal and decreased kurtosis as frequency increased in simulations of two-compartment tissues [17]. In contrast, similar to our results, no significant difference was observed in the b-value dependence measurement using the agarose gel phantom [21]. NMR diffusion measurements in yeast cells suggest that at diffusion times <10 ms, the b-value settings reflect the biophysical characteristics of cell organelles such as nuclei and vacuoles as well as the intra- and extracellular levels [18]. A previous study [22] that investigated the mouse brain using OGSE confirmed the frequency dependence of diffusion coefficients, thereby suggesting a more selective observation of complex diffusion phenomenon in vivo by setting the frequency.

OGSE requires a high gradient strength and slew rate due to the large gradient shifts between positive and negative peaks. Therefore, the b-value and the upper limit of frequency change based on the gradient performance. In addition, frequency is limited by the phase of the applied waveform [23]. For OGSE measurements, the modulation gradient varies depending on the performance of the device and the applied waveform. Hence, the characteristics are challenging to evaluate uniformly. To measure complex biological structures using OGSE, as performed in previous studies [15,19,21,22,26], simple structures, such as phantoms, are evaluated under

the same sequence conditions for imaging biological tissue and compared for the accurate evaluation of the transitional characteristics of diffusion coefficients.

Previous studies [5,6,17] using fiber phantoms and bead-filled phantoms have shown that OGSE is superior at detecting complex shapes of structural walls and extra-axonal spaces than estimating axonal inner diameters. OGSE has been applied to the preliminary assessment of glioblastoma [15] and observing alterations in brain cell structure with ischemic stroke [13]. Diffusion NMR measurements with finite pulse gradient [32] or modulated gradient spin echo [33] provide information related to microporous structures. Similar to these NMR-porosity measurements, OGSE could also be a tool for noninvasive imaging of the diffusion properties of microporous structures. This study investigated the OGSE diffusion characteristics inside a restricted structure using a capillary phantom. Results showed that OGSE is superior to PGSE in detecting microstructural displacements at the micron scale, even for intrastructural diffusion. This finding supports the notion that OGSE is an effective tool for detecting displacement on the mesoscopic scale, both inside and outside the structure.

5. Conclusion

The restricted diffusion characteristics of each OGSE-applied waveform with different b-values and frequencies (N) were investigated using several sizes of capillary plates. The sine wave measurement could obtain diffusion information similar to PGSTE. Hence, in the cosine measurement, a higher frequency (N) captures faster diffusion within the diffusion phenomena.

CRediT authorship contribution statement

Hinako Oshiro: Writing – review & editing, Writing – original draft, Methodology, Investigation, Formal analysis, Data curation, Conceptualization. **Junichi Hata:** Writing – review & editing, Writing – original draft, Supervision, Project administration, Methodology, Investigation, Funding acquisition, Formal analysis, Data curation, Conceptualization. **Daisuke Nakashima:** Writing – review & editing, Investigation. **Rintaro Oshiro:** Writing – review & editing, Investigation, Formal analysis, Data curation. **Naoya Hayashi:** Writing – review & editing, Investigation. **Yawara Haga:** Writing – review & editing, Investigation. **Kei Hagiya:** Writing – review & editing, Investigation. **Daisuke Yoshimaru:** Writing – review & editing, Investigation. **Hideyuki Okano:** Writing – review & editing, Supervision, Funding acquisition.

Declaration of competing interest

The authors declare that they have no known competing financial interests or personal relationships that could have appeared to influence the work reported in this paper.

Acknowledgments

This work was supported by the program for Brain Mapping by Integrated Neurotechnologies for Disease Studies (Brain/MINDS) from the Japan Agency for Medical Research and Development (AMED) (Grant Number JP15dm0207001 to H.O.), JSPS KAKENHI (Grant Number JP20H03630 to J.H.), and “MRI platform” (Grant Number JPMXS0450400622 to J.H.) as a program of Project for Promoting public Utilization of Advanced Research Infrastructure of the Ministry of Education, Culture, Sports, Science and Technology (MEXT), Japan. We thank Araki Rikita, Bruker Japan, for support with MRI systems.

Appendix A. Supplementary data

Supplementary data to this article can be found online at https://doi.org/10.1016/j.heliyon.2024.e26391.

References

[1] E.O. Stejskal, J.E. Tanner, Spin diffusion measurements: spin echoes in the presence of a time-dependent field gradient, J. Chem. Phys. 42 (1965) 288–292.
[2] P.J. Basser, J. Mattiello, D. LeBihan, Estimation of the effective self-diffusion tensor from the NMR spin echo, J. Magn. Reson. 103 (1994) 247–254.
[3] Y. Assaf, T. Blumenfeld-Katzir, Y. Yovel, P.J. Basser, AxCaliber: a method for measuring axon diameter distribution from diffusion MRI, Magn. Reson. Med. 59 (2008) 1347–1354.
[4] I. Drobnjak, H. Zhang, A. Ianuş, E. Kaden, D.C. Alexander, PGSE, OGSE, and sensitivity to axon diameter in diffusion MRI: Insight from a simulation study, Magn. Reson. Med. 75 (2016) 688–700.
[5] L.M. Burcaw, E. Fieremans, D.S. Novikov, Mesoscopic structure of neuronal tracts from time-dependent diffusion, Neuroimage 114 (2015) 18–37.
[6] D.S. Novikov, E. Fieremans, S.N. Jespersen, V.G. Kiselev, Quantifying brain microstructure with diffusion MRI: theory and parameter estimation, NMR Biomed. 32 (2019) 1–53.
[7] J. Stepišnik, Time-dependent self-diffusion by NMR spin-echo, Phys B Phys Condens Matter 183 (1993) 343–350.
[8] L.L. Latour, K. Svoboda, P.P. Mitra, C.H. Sotak, Time-dependent diffusion of water in a biological model system, Proc Natl Acad Sci U S A 91 (1994) 1229–1233.
[9] M. von Smoluchowski, Zur kinetischen Theorie der Brownschen Molekularbewegung und der Suspensionen, Annal Phys 326 (1906) 756–780.
[10] F. Grussu, K. Bernatowicz, I. Casanova-Salas, et al., Diffusion MRI signal cumulants and hepatocyte microstructure at fixed diffusion time: Insights from simulations, 9.4 T imaging, and histology, Magn. Reson. Med. 88 (2022) 365–379.

[11] P. Porcari, M.G. Hall, C.A. Clark, et al., The effects of ageing on mouse muscle microstructure: a comparative study of time-dependent diffusion MRI and histological assessment, NMR Biomed. 31 (2018) 1–13.
[12] D.S. Novikov, J.H. Jensen, J.A. Helpern, E. Fieremans, Revealing mesoscopic structural universality with diffusion, Proc Natl Acad Sci U S A 111 (2014) 5088–5093.
[13] T.X. Cai, N.H. Williamson, V.J. Witherspoon, R. Ravin, P.J. Basser, A single-shot measurement of time-dependent diffusion over sub-millisecond timescales using static field gradient NMR, J. Chem. Phys. 154 (2021) 111105.
[14] M. Schachter, M.D. Does, A.W. Anderson, J.C. Gore, Measurements of restricted diffusion using an oscillating gradient spin-echo sequence, J. Magn. Reson. 147 (2000) 232–237.
[15] J.C. Gore, J. Xu, D.C. Colvin, et al., Characterization of tissue structure at varying length scales using temporal diffusion spectroscopy, NMR Biomed. 23 (2010) 745–756.
[16] E.C. Parsons, M.D. Does, J.C. Gore, Temporal diffusion spectroscopy: theory and implementation in restricted systems using oscillating gradients, Magn. Reson. Med. 55 (2006) 75–84.
[17] S. Portnoy, J.J. Flint, S.J. Blackband, G.J. Stanisz, Oscillating and pulsed gradient diffusion magnetic resonance microscopy over an extended b-value range: Implications for the characterization of tissue microstructure, Magn. Reson. Med. 69 (2013) 1131–1145.
[18] W. Mazur, A.T. Krzyżak, Attempts at the characterization of in-cell biophysical processes non-invasively-quantitative NMR diffusometry of a model cellular system, Cells 9 (2020) 1–17.
[19] C.A. Baron, C. Beaulieu, Oscillating gradient spin-echo (OGSE) diffusion tensor imaging of the human brain, Magn. Reson. Med. 72 (2014) 726–736.
[20] N. Pyatigorskaya, D. Le Bihan, O. Reynaud, L. Ciobanu, Relationship between the diffusion time and the diffusion MRI signal observed at 17.2 tesla in the healthy rat brain cortex, Magn. Reson. Med. 72 (2014) 492–500.
[21] D. Wu, J. Zhang, The effect of microcirculatory flow on oscillating gradient diffusion MRI and diffusion encoding with dual-frequency orthogonal gradients (DEFOG), Magn. Reson. Med. 77 (2017) 1583–1592.
[22] M. Aggarwal, M.D. Smith, P.A. Calabresi, Diffusion-time dependence of diffusional kurtosis in the mouse brain, Magn. Reson. Med. 84 (2020) 1564–1578.
[23] E.T. Tan, R.Y. Shih, J. Mitra, et al., Oscillating diffusion-encoding with a high gradient-amplitude and high slew-rate head-only gradient for human brain imaging, Magn. Reson. Med. 84 (2020) 950–965.
[24] C. Pierpaoli, P.J. Basser, Toward a quantitative assessment of diffusion anisotropy, Magn. Reson. Med. 36 (1996) 893–906.
[25] H. Oshiro, J. Hata, D. Nakashima, et al., Influence of diffusion time and temperature on restricted diffusion signal: a phantom study, Magn. Reson. Med. Sci. (2023). https://www.jstage.jst.go.jp/article/mrms/advpub/0/advpub_mp.2022-0103/_article/-char/en.
[26] M.D. Does, E.C. Parsons, J.C. Gore, Oscillating gradient measurements of water diffusion in normal and globally ischemic rat brain, Magn. Reson. Med. 49 (2003) 206–215.
[27] M. Holz, S.R. Heil, A. Sacco, Temperature-dependent self-diffusion coefficients of water and six selected molecular liquids for calibration in accurate 1 H NMR PFG measurements, Phys. Chem. Chem. Phys. 2 (2000) 4740–4742.
[28] T.G. Reese, O. Heid, R.M. Weisskoff, V.J. Wedeen, Reduction of eddy-current-induced distortion in diffusion MRI using a twice-refocused spin echo, Magn. Reson. Med. 49 (2003) 177–182.
[29] K. Borkowski, A.T. Krzyżak, The generalized Stejskal-Tanner equation for non-uniform magnetic field gradients, J. Magn. Reson. 296 (2018) 23–28.
[30] A.T. Krzyzak, Z. Olejniczak, Improving the accuracy of PGSE DTI experiments using the spatial distribution of b matrix, Magn. Reson. Imaging 33 (2015) 286–295.
[31] A. Krzyzak, K. Borkowski, Theoretical analysis of phantom rotations in BSD-DTI, Annu Int Conf IEEE Eng Med Biol Soc 2015 (2015) 410–413.
[32] J. Stepišnik, B. Fritzinger, U. Scheler, A. Mohorič, Self-diffusion in nanopores studied by the NMR pulse gradient spin echo, Epl 98 (2012) 57009.
[33] J. Stepišnik, I. Ardelean, A. Mohorič, Molecular self-diffusion in internal magnetic fields of porous medium investigated by NMR MGSE method, J. Magn. Reson. 328 (2021) 106981.